The Global Surface Roughness of 433 Eros from the NEAR Laser Rangefinder

Hannah C. M. Susorney[a,b], Olivier S. Barnouin[c,d]

[a] *Department of Earth and Planetary Science, The Johns Hopkins University, Baltimore, MD 21218, USA.*
[b] *Department of Earth, Ocean and Atmospheric Sciences, University of British Columbia, Vancouver, BC 21218, USA.*
[c] *The Johns Hopkins University Applied Physics Laboratory, Laurel, MD 20723, USA.*
[d] *Hopkins Extreme Material Institute, The Johns Hopkins University, Baltimore, MD 21218, USA.*

Abstract

We performed the first global surface roughness assessment of the asteroid 433 Eros at baselines (horizontal distances) of 4–200 m. We measured surface roughness using the root-mean-square (RMS) deviation over a variety of baselines after first detrending the height to remove long-wavelength slope effects. The global surface roughness of Eros is found to be self-affine at all baselines investigated. The surface roughness is statistically correlated with crater density at baselines of 100–200 m and boulders at a baseline of 5 m. No global spatial statistical correlation was found for baselines of 4–200m and mapped tectonic lineaments, ponds, slope, or geopotential elevation. The surface roughness of the crater Shoemaker (Charlois Regio) is controlled by the interplay of a high boulder density producing higher surface roughness values at small baselines and low crater density lowering surface roughness values at long baselines. We estimated the mobile regolith thickness (regolith that moves around and infills topography) to be 0.2–6.2 m from the difference in the surface roughness values at the baseline of 4 m. Furthermore, we find that the change in RMS deviation as a function of baseline compares favorably with the moon, and differs significantly from existing results for rubble-pile asteroid Itokawa.

Keywords: Asteroids, Topography, 433 Eros, Boulders, Impact Craters

1. Introduction

Surface roughness is a statistical measure of the change in topography over a specified horizontal scale after removing a trend (Shepard et al., 2001). Studies of the surface roughness of asteroids can be divided into two classes based on the horizontal scale of surface roughness. The majority of asteroid studies focus on centimeter-scale surface roughness derived from radar studies (e.g. Benner et al., 2008) and thermal modeling (e.g., Harris and Lagerros, 2002). The other class of studies focuses on the surface roughness estimated at horizontal scales $>$ 1-meter using measured asteroid topography (Cheng et al., 2001, 2002; Abe et al., 2006; Barnouin-Jha et al., 2008). The latter studies use scales similar to those used for evaluating surface roughness on larger planetary bodies such as Mars, Moon, and Mercury (Garvin et al., 1999; Rosenburg et al., 2011; Kreslavsky et al., 2014) and permit statistical comparisons between asteroids and planetary bodies. Meter-scale surface roughness studies require accurate topography of asteroids with vertical resolutions that are at least a factor of 10 better than the horizontal scales over which the roughness is evaluated. Such high-quality topography is available from robotic missions to asteroids when they include laser altimeters (i.e., Near Earth Asteroid Mission, NEAR, Shoemaker to 433 Eros and Hayabusa to 25143 Itokawa), or when they include extensive imaging with high spatial resolutions. This study focuses on surface roughness measured at horizontal scales ranging from 4–200 m on the asteroid 433 Eros (hereafter called Eros) using the NEAR Laser Rangefinder (NLR) altimetric data.

Eros is a large elongate 30 x 15 x 15 km asteroid with a density of 2.67 ± 0.1 g/cm^3 (Veverka et al., 2000), a porosity of 20–25 %, and is likely a fractured shard (Wilkison et al., 2002). Previous studies of the surface roughness of Eros measured the meter-scale surface roughness from individual NLR tracks for specific regions across the asteroid (Cheng et al., 2001, 2002). The highest surface roughness values were found within the 5 km-diameter crater Psyche, specifically on Psyche's rim and walls, where boulders are common. Regions near the Rahe-Dorsum of Eros, a large fault with associated surface lineaments, was also associated with higher surface roughness values.

The surface roughness of 25143 Itokawa for a few regions,(Abe et al., 2006; Barnouin-Jha et al., 2008) was obtained from a laser altimeter using a smaller range of horizontal baselines (5–100 m) than measured on Eros. 25143 Itokawa (hereafter called Itokawa) is a small elongated (0.55 x 0.3 x 0.25 km) rubble-pile asteroid (Fujiwara et al., 2006) with two terrain types: lowlands that have lower surface roughness values than Eros and highlands that have similar surface roughness values to Eros (Abe et al., 2006; Barnouin-Jha et al., 2008). The difference in surface roughness values between the two regions is due to the higher density of boulders in the highlands. If, as imaging suggests, (Miyamoto et al., 2007) the lowlands were previously covered in boulders and were buried by regolith, the difference in surface roughness at smaller baselines could provide a lower bound estimate of regolith thickness on Itokawa. Using this methodology, Barnouin-Jha et al. (2008) found a lower bound estimate of regolith thickness for Itokawa of 2.3 ± 0.4 m. In all of the previous studies of the meter-scale surface roughness of asteroids the topography was not detrended to remove pre-existing large-scale topography before the surface roughness measurements were performed, although areas on Itokawa were chosen to have low slopes (Abe et al., 2006; Barnouin-Jha et al., 2008).

While these studies provide valuable insight into the surface properties of Eros and Itokawa for specific regions none of them include a global assessment of surface roughness as has been done for larger planetary bodies (e.g., Kreslavsky and Head, 2000; Rosenburg et al., 2011). In this study, we measure the global meter-scale surface roughness of Eros. Global surface roughness maps can provide inferences on which geologic processes influence regional topography to modify the asteroid's surface roughness. Candidate processes for Eros include impact cratering (e.g., Chapman et al., 2002), formation of lineaments (e.g., Buczkowski et al., 2008), regolith processes and boulder mobilization (e.g., Thomas et al., 2002), and the creation of ponds (e.g., Robinson et al., 2001). Many of these processes have been cited as key contributors to changes in surface roughness on other bodies including cratering on the Moon (Rosenburg et al., 2011), and tectonics and cratering on Mercury (Kreslavsky et al., 2014; Susorney et al., 2017).

We use root-mean-square, RMS, deviation (the RMS of the difference in detrended height over a specified horizontal scale) as our measure of surface roughness for several reasons. First, RMS deviation is widely used in surface roughness investigations of asteroids using radar (e.g., Benner et al., 2008) and thermal datasets (e.g., Harris and Lagerros, 2002). Additionally, RMS deviation has been used in previous investigations of the surface roughness of asteroids (Cheng et al., 2001; Barnouin-Jha et al., 2008) and in investigations of larger planetary bodies (e.g., Rosenburg et al., 2011) allowing us to compare our data to previous studies. Second, RMS deviation is frequently used to model topography of a surface as a self-affine fractal if RMS deviation scales with a given length-scale (or baseline) as a power law with a constant exponent, known as the Hurst exponent [Turcotte, 1997]. A single diagnostic Hurst exponent [Shepard et al., 2001] for a surface could indicate that topography is the result of a single geologic process that operates at many scales. A break in the slope of RMS deviation at a given baseline (i.e., a change in Hurst exponent) may imply that more than one process is playing a role in influencing the observed topography, usually with one process influencing shorter baselines and another affecting longer baselines. Finally, RMS deviation is a straight-forward measurement easing interpretation of surface roughness maps.

This study presents the first global maps of surface roughness of an asteroid with baselines ranging from 4–200 m. We break the study into five parts, beginning with a discussion of the methodology employed to calculate and grid surface roughness measurements across Eros. This is not as straightforward as previous global surface roughness assessments on planets given the irregular and elongate shape of Eros. We present our resulting global surface roughness maps projected onto a shape model of 433 Eros and discuss the extent to which the surface roughness is correlated with various geologic features. We complete our efforts by discussing the geology of Eros in terms of the measured surface roughness, which, as on Itokawa, can provide an estimate of the mobile portion of the regolith on Eros.

In this study, we use common names in the literature for the largest crater on Eros (see Fig. 1). The crater Shoemaker (12°S 25°E, called Charlois Regio by the International Astronomical Union, IAU), is the youngest crater of the three discussed here and is 7.6 km in diameter (Thomas et al., 2001). Shoemaker overlaps the crater Himeros (5°N 75°E), which is 10 km in diameter. Psyche (15°N 275°E) is on the opposite side of Eros and is 5.3 km in diameter. The naming convention for Charlois Regio/Shoemaker in this paper is used for consistency with previous studies (e.g., Cheng et al., 2002; Buczkowski et al., 2008) and for the rest of the paper we will refer to Charlois Regio as Shoemaker crater.

2. Methodology

We used topography data (Fig. 1) for Eros from the NLR instrument that flew aboard the NEAR-Shoemaker spacecraft (Zuber et al., 1997). NLR collected over 16 million returns while in orbit around Eros from February 2000 to February 2001 (Cheng et al., 2002). Individual NLR transects or tracks are composed of a series of altimetric returns collected as the spacecraft traveled forward. We use these individual NLR tracks instead of derived topography in the form of digital terrain maps (DTMs) that are available for NLR data. DTMs are often generated by binning and interpolating the altimetric data (see discussion in Glaze et al., 2003; Barnouin-Jha et al., 2005). Making use of individual altimetry tracks is particularly important for NLR data collected at Eros because radial spacecraft trajectory uncertainties could result in differences of up to 100 m between individual NLR tracks, although on average they differ by a RMS value of 22 m (Miller et al., 2002; Kahn et al., 2015). Additionally, the precision of individual NLR returns is 0.312 m (Cheng et al., 2002) and we use this value as our precision for surface roughness measurements. During binning for DTM production, these uncertainties can influence the inferred surface shape. In such situations, it is desirable to measure roughness along individual NLR tracks, where the topography measured is self-consistent. The penalty for using NLR data, rather than DTMs derived from NLR or imaging is that the density of NLR data across Eros is non-uniform leading to some loss of spatial coverage. However, this lack of spatial coverage is traded against higher accuracy surface roughness measurements derived from the higher precision NLR data.

We measured surface roughness using RMS deviation as has been done in previous studies of the meter-scale surface roughness of asteroids (Cheng et al., 2001, 2002; Abe et al., 2006; Barnouin-Jha et al., 2008). We calculated RMS deviation using methodology from Susorney et al. (2017), but modified to take into account the complex, non-ellipsoid, 3-dimensional geometry of Eros. Topography was detrended at ten-times the horizontal scale (baseline) used for estimating surface roughness before surface roughness calculations were made. This detrending removed broad-scale topography following the recommendations of Shepard et al. (2001). In what follows, we discuss the nature of the NLR data and define RMS deviation. Furthermore, we present how we processed and filtered the NLR data when computing RMS deviation, and show how the results are gridded and mapped across the asteroid. We also explain the derivation of the Hurst exponents for Eros.

2.1. NLR data

The NLR instrument operated continuously while the NEAR spacecraft was in orbit. The distances between individual NLR footprints (Fig. 2) was primarily a function of the orbital speed and distance to the surface of Eros (Zuber et al., 2000). Fig. 2a shows that the majority of NLR points are less than 4 m apart and we used this value as our smallest baseline for surface roughness measurements. We used a maximum baseline of 200 m because we needed to detrend the track over a spatial scale 10 times the baseline of interest and the tracks used were only several kilometers long for reasons presented below.

A combination of NEAR-Shoemaker orbits, the shape of Eros, and changes in spacecraft pointing was such that many NLR tracks are not straight lines across the surface of Eros. The methodology we employ for measuring the distance between returns and detrending the NLR data requires the tracks to be as straight as possible for best results in estimating the distance between NLR returns. We filtered the NLR tracks to 'cut' them at points when the tracks changed in direction using an automated methodology. We looked for abrupt changes in NLR track longitude. This method was conservative and resulted in shorter NLR tracks, but a more reliable horizontal distance estimates between NLR points and detrend the data appropriately.

2.2. RMS deviation

RMS deviation [$\nu(L)$] is the root-mean-square (RMS) of the change in topography over a baseline (Shepard et al., 2001). It is defined as the following,

$$\nu(L) = \left\{ \frac{1}{n} \sum_{i=1}^{n} [\Delta h(L)_i]^2 \right\}^{\frac{1}{2}}, \tag{1}$$

where $\Delta h(L)$ is the change in height over a given baseline, L, and n is the number of Δh used in the calculation of RMS deviation. $\nu(L)$ is known fluctuate below a threshold value of n for planetary surfaces (Kreslavsky et al., 2013; Shepard et al., 2001; Rosenburg et al., 2011; Susorney et al., 2017), Fig. 2b shows the stability of the estimate of $\nu(L)$ for a single location on Eros. From analyzing many locations on Eros, we found RMS deviation becomes stable when $n \sim 200$; similar to results for Mercury (Susorney et al., 2017). Therefore, we use a minimum of 200 Δh when calculating $\nu(L)$.

2.3. NLR track filtering and surface roughness calculation

Calculating $\nu(L)$ from NLR tracks cannot be done in the same manner as for planets due to the irregular shape of 433 Eros. We expanded upon a methodology for uneven track spacing developed in Susorney et al. (2017), but adapt it for the 3-dimensional geometry of an asteroid. We start by using individual 'cut' NLR tracks and then calculate the geopotential elevation (i.e., topography) from a geoid generated from an NLR track-derived shape model, assuming a homogeneous distribution of mass with a density of 2.67 g/cm^3 and a rotation rate of 0.000331 radians/second (Abe et al., 2006). We use topography rather than surface shape since, for irregular bodies, the surface shape and topography can differ dramatically.

We evaluated each NLR point on each track to calculate Δh. Then we calculated the 'true' distance between NLR points on the 'cut' tracks within 500 m (measured as a straight-line distance) of the NLR point being investigated using a modification of the methods outlined in Cheng et al. (2001, 2002) and Barnouin-Jha et al. (2008). The distance was calculated by fitting the x, y, and z coordinates of the NLR track as a straight-line function of time, to capture some of the curvature of Eros. We measured the distance between returns along this line. Once we calculated distance, we found all the points within $5L$ on either side of the point. We then linearly interpolated the NLR points to produce topography with the spacing of L and then detrended the interpolated track 10 L . In Susorney et al. (2017) interpolated tracks were compared to tracks without interpolation and no statistical difference in surface roughness was found between both methodologies. Finally, the Δh from the two adjacent topography points was measured. This methodology was repeated for all NLR points at all baselines.

2.4. Shape model gridding

The gridding and projecting of surface roughness maps were done on a 3-dimensional shape model of Eros. We used the 3-dimensional shape model to avoid the distortion of projecting an irregular object unto a map designed for a sphere. For our maps, we degraded a shape model of Eros (Gaskell, 2008) into a 2000 plate model so that we had sufficient Δh for each plate. On average, the surface area of each plate is 0.562 km^2, making each plate about 0.05 % of the total surface area of the asteroid. For each L, all Δh values within $2L$ and $\nu(L)$ were calculated using Equation 1. If less than 200 Δh values were present, we did not calculate $\nu(L)$ and the plate is represented as a gray plate in our maps.

2.5. Hurst exponent

RMS deviation is related to the self-affine nature of many planetary surfaces through a value called the Hurst exponent, H. The Hurst exponent can be measured if the surface roughness when plotted as the log of RMS deviation versus the log of baseline (the plot is called a deviogram) is a straight line (Turcotte, 1997; Shepard et al., 2001). The Hurst exponent is defined as the following,

$$\nu(L) = \nu_o L^H, \tag{2}$$

where ν_o is the RMS deviation at the unit scale, m, (Shepard et al., 2001). We estimate H for each plate, for the entire asteroid, and for Shoemaker crater.

3. Results

In this section, we present 3-dimensional shape models with the RMS deviation calculated for each plate. We discuss 'small-scale' , L = 4–10 m, 'medium-scale' , L = 20–90 m, and 'large-scale' , L = 100–200 m baselines separately. We present a representative map for each category. A map of the Hurst exponents for each plate and a global deviogram is also shown. The different baseline categories and representative maps were chosen to highlight different spatial variations in surface roughness found in each baseline category.

3.1. Small-scale roughness 4-10 m

At L = 5m (Fig. 3), there are high surface roughness values in the three largest craters on the surface (Psyche, Himeros, and Shoemaker). The largest spatial region of elevated roughness values is in Shoemaker, the youngest crater of the three (Thomas et al., 2001).

3.2. Medium-scale roughness 20-100 m

At the $L = 50$ m baseline (Fig. 4), the three largest craters have slightly elevated surface roughness values, but to a lesser degree than in the small-scale maps.

3.3. Large-scale roughness 100-250 m

At the largest baselines (Fig. 5) the surface roughness values are lowest in the large craters Himeros and Shoemaker. A band of lower surface roughness values wraps around the southern edge of Himeros and Shoemaker continuing around the nose to the north. The crater Psyche's surface roughness values are indistinguishable from surrounding surface roughness values.

3.4. Deviogram and Hurst exponents

Deviograms for the entire surface of 433 Eros and the crater Shoemaker are shown in Fig 6. The surface of Eros is self-affine with an overall Hurst exponent of 0.97 ± 0.01. The ν_o of Eros is 0.14 ± 0.01 m. The deviogram for the crater Shoemaker shows the observed trend of Shoemaker having higher surface roughness values than the rest of Eros at small baselines and lower surface roughness values than the rest of Eros at large baselines as seen in Figs 3-5.

A map of the Hurst exponent calculated for each plate is shown in Fig 7. The Hurst exponent is lowest in the craters Shoemaker and Himeros and is close to ~ 1 in the crater Psyche.

4. Geologic Processes and Surface Roughness

In this section, we focus on relating the observed surface roughness on Eros to various geologic processes. The boulder and crater counts used in the following section were kindly provided by P.C. Thomas (Thomas et al., 2002; Thomas and Robinson, 2005).

4.1. Boulders

The highest density of boulders ($>$ 16 m in diameter, Fig. 9) is found in Shoemaker crater. A positive weak (r = 0.21) but statistically significant correlation (p = 1.4e-05) can be found across the entire surface of the asteroid between the surface roughness computed at $L = 5$ m and boulder density when a given plate of the low resolution 2000-plate Eros shape model has more than 15 boulders present. We calculated a Pearson correlation coefficient for all of our correlation tests with an N of 2000 (for the 2000 plate model) and assumed the results were statistically significant if p was less than 0.05. Given that for many regions of Eros there is a deficit of craters under 100 m in diameter (Chapman et al., 2002) especially in Shoemaker crater (Thomas and Robinson, 2005), and evidence for the presence of boulders in images, the correlation result is consistent with boulders providing the main contributions to surface roughness measured at small baselines on Eros.

4.2. Cratering

The lowest density of impact craters (177 - 1000 m in diameter, Fig. 8) is found in Shoemaker and Himeros craters, which corresponds to the lowest surface roughness values at long baselines. The band of low surface roughness values around the craters Himeros and Shoemaker (a region of low surface roughness values at L = 100–200 m, Fig. 5) corresponds to a region of low crater density (Fig. 8). We found a positive weak correlation (r = 0.44) between surface roughness at 100 m and impact crater density and a positive moderate correlation (r = 0.54) at 200 m, both correlations were statistically significant(p = 1.8e-22 and 9.6e-30 respectively).

4.3. Tectonics

The surface of Eros is covered in structural lineaments (Buczkowski et al., 2008). Past studies of the surface roughness of Eros noted that the surface roughness values from individual NLR tracks increased at structural lineaments (Cheng et al., 2002). We checked for a correlation between the density of lineaments that intersected a plate and surface roughness at baselines of 4 - 200 m and no statistical correlation was found. We also checked for any visual correlation between the maps and did not observe any correlation.

4.4. Ponds

Ponds are nearly flat deposits on asteroids such as Eros whose origin is debated (Roberts et al., 2014). In images, ponds appear smooth down to 1.2 cm per pixel resolution (Robinson et al., 2001). While these ponds have been described as qualitatively smooth (e.g., Robinson et al., 2001) no quantitative study of their surface roughness has been performed. Ponds range in size from 7–210 m, the scale of our roughness measurements (Robinson et al., 2001; Thomas et al., 2002; Roberts et al., 2014). We checked for a correlation with our global surface roughness measurements with a map of pond density generated from Roberts et al. (2014) at L = 5, 10, and 20 m. We found no correlation with surface roughness and pond density. This is not surprising given the relatively small size and number of ponds. They do not significantly influence the global surface roughness of Eros at baselines we measured.

4.5. Slope and Geopotential Elevation

We investigated the possibility of correlations between slope and geopotential elevation and surface roughness. In Cheng et al. (2002) a visual correlation was found between regions of high slope and regions of high surface roughness. We calculated the slope and geopotential elevation for a 49,152 plate shape model of Eros and used his data to calculate the average slope and geopotential elevation for our degraded 2000 plate model. We looked for a correlation with slope and geopotential elevation for all of the baselines measured here and found none.

5. Discussion

5.1. Geologic processes on Eros and surface roughness

The surface roughness of Eros is dominated by two main geologic features: impact craters and boulders. Impact crater density is correlated with surface roughness above 100 m, consistent with previous observations for larger planetary bodies including the Moon (Rosenburg et al., 2011) and Mercury (Kreslavsky et al., 2014; Fa et al., 2016; Susorney et al., 2017). Boulder density is statistically correlated with the global surface roughness of Eros at the baseline of 5 m.

The distribution of large boulders and small to intermediate sized craters on Eros is linked to the most recent large impact on the surface (the formation of Shoemaker and subsequent seismic shaking from the impact) (Thomas and Robinson, 2005). A deficit of impact craters near the impact site (seen in the low surface roughness density at long baselines) and a deficit of craters in straight-line distance from the crater center (representing travel time for seismic waves) are proposed to be due to seismic shaking (Thomas and Robinson, 2005). The boulder density also follows the expected ejecta distribution from the Shoemaker impact (Thomas et al., 2001), which is correlated to the surface roughness at $L = 5$ m. While the boulder and crater distributions are different they are linked by the formation of the crater Shoemaker.

Previous studies of localized surface roughness on Eros have identified lineaments as sources of high surface roughness values (Cheng et al., 2002). We did not see evidence of correlations between maps of the density of tectonic lineaments and maps of surface roughness. The lack of correlation may be due to two factors: the need for large plates (required to keep RMS deviation from fluctuating) in mapping surface roughness and the relatively localized nature of lineaments. Further, lineaments do not generate substantial topography, meaning they are unlikely to be the source of surface roughness to the same extent as boulders and craters.

The rim of Psyche was found to have higher surface roughness values than the crater walls in a previous study of the surface roughness of Eros (Cheng et al., 2002) at all L measured (5–1000 m). This observation may be due to not detrending the topography before calculating surface roughness and thus previous measures of surface roughness of Eros may have been measuring the slope rather than the surface roughness. However, some regions (plates) within Psyche possess higher surface roughness relative to the rim in our study ($L = 50$ m). Cheng et al. (2002) proposed that such higher surface roughness values on the crater wall were indicative of exposure of bedrock. Cheng et al. (2002) also noted higher surface roughness values near high slopes and this was also interpreted as evidence of exposure of bedrock. It was postulated that on high slopes regolith could have slid off the slopes, and exposed bedrock with higher surface roughness values. We could not find a significant correlation between surface roughness and slope. If there is an increase in surface roughness values on slopes it is not a global enough phenomena that a global map would detect it. It could also simply mean that bedrock (if exposed) is similar in surface roughness to regolith or that no bedrock is exposed. We can compare the measurements of Eros' surface roughness to past studies of surface roughness from Eros and other bodies (Table. 1) and find that our values for the surface roughness of Eros are higher than previous studies. This could be due to including the global dataset in our calculations (including smoother regions that were not studied previously) and updated methodologies.

5.2. Regolith

For small baselines on Eros (under 10 m) boulders are the likely source of variations in surface roughness consistent with previous studies of Eros and Itokawa (Cheng et al., 2001, 2002; Abe et al., 2006; Barnouin-Jha et al., 2008). This observation was used on Itokawa to estimate a lower bound on regolith thickness (Barnouin-Jha et al., 2008) due to the evidence that regolith appears to cover boulders and embays the lowland (Miyamoto et al., 2007; Barnouin-Jha et al., 2008). Other evidence for regolith mobility on Itokawa includes the imbrication of adjacent boulders in the direction of slope (Miyamoto et al., 2007).

Eros has a layer of tens of meters of regolith that has covered boulders to varying degrees (Fig. 11) and is mobile as seen by the flat floors at the bottom of some craters (Veverka et al., 2001; Robinson et al., 2002; Dombard et al., 2010) and imbrication of boulders (Barnouin et al., 2012). If small-scale surface roughness ($L = 5$ m) is due primarily to regolith covering boulders and infilling other changes in topography (Fig 10) we can derive a lower limit on regolith thickness from the difference in surface roughness measurements at small baselines for different regions of Eros. This assumes that at times in the past boulders covered all of Eros, but we believe this is likely because of the Eros has several large craters that must have left behind large populations of boulders strewn across the asteroid. This was observed on Lutetia by Thomas et al. (2012), for example, where each crater left behind boulders around all the large observed craters. We estimated the thickness of mobile regolith that could cover older boulders by comparing the 1st and 3rd quartile of RMS deviation from the 2000 plate model at $L = 5$ m and found the difference in surface roughness to be 0.2 m. The difference in maximum surface roughness value and minimum surface roughness at $L = 5$ m is 6.2 m. This produces a range in mobile regolith for Eros of 0.2–6.2 m, less than estimates for total regolith thickness of Eros (Veverka et al., 2001; Robinson et al., 2002) derived from infilled craters, but similar to estimates for Itokawa (2.3 ± 0.4) (Barnouin-Jha et al., 2008).

This estimate of the thickness of the mobile regolith possess does not take into account other processes that could alter the assumptions made. For example processes such as shaking-induced assortment, the "Brazil nut effect' which causes larger particles to reach the surface (e.g., Murdoch et al., 2015).

We believe this effect is probably not very important on Eros, where many blocks (other than the ones directly linked to Shoemaker crater formation) tend to be located at local slope minima, near the bottom of craters. Maybe of bigger concern than the brazil nut effect, is the assumption that boulders evenly covered the surface after the formation of the many large craters on Eros, and that they were not intimately mixed with finer regolith as might be expected for ejecta deposits. The evidence presented previously for Lutetia, as well as observation of small lunar craters (Krishna and Kumar, 2016), indicates that it is very likely blocks are often the last ejecta components that fall on top of the finer ejecta. So while some caveats exist, our roughness assessment suggest some evidence for a mobile regolith layer that is on the order of 0.2 to 6.2 m that reduces surface roughness values by covering existing blocks with finer materials.

5.3. Comparisons of Eros to other planetary bodies

Deviograms provide a quantitative way to compare the surface roughness on different bodies where similar baselines of surface roughness have been measured. In Fig. 6, we compare Eros to a deviogram of the Moon [calculated for this study, using the same methodology in Susorney et al. (2017)] for a region of the lunar mare and lunar highlands. Both the lunar highlands and mare are smoother than Eros possibly due to the retention of more ejecta on the moon, which infills topography producing a smoother surface. Two deviograms of the surface roughness of Itokawa (Barnouin-Jha et al., 2008) are also shown in Fig. 6. The lowlands of Itokawa (Muses-C) have lower surface roughness values than the global Eros deviogram at the same baselines and the highlands of Itokawa match the global surface roughness values of Eros. A caveat to comparing Barnouin-Jha et al. (2008) to our study is that Barnouin-Jha et al. (2008) did not detrend topography before calculating surface roughness, although they used flat regions. The similarity of values of Eros and the highlands of Itokawa is likely due to the presence of blocks on both Eros and the highlands of Itokawa.

Eros and the Moon have similarly shaped deviograms and are both self-affine. Itokawa is not self-affine and the deviogram is flat (Barnouin-Jha et al., 2008). The similarity in deviogram shape between the Moon and Eros and the difference in deviogram shape between Eros and Itokawa imply that the subsurface of Eros has strength and can support topography (unlike Itokawa, a rubble-pile). This implies that the shape of the deviogram may be diagnostic of the interior structure of asteroids. Future measurements of the meter-scale surface roughness of asteroids will allow us to explore this relationship between deviogram shape and sub-surface structure.

The Hurst exponent of the lunar highlands and the mare are 0.95 and 0.76 respectively for baselines of 17–2700 m (Rosenburg et al., 2011). The Hurst exponent for Mercury's cratered terrain is 0.95 ± 0.01 for baselines of 500–1500 m (Susorney et al., 2017). Both the lunar highlands (the more heavily cratered region of the moon) and the mercurian cratered terrain (the more heavily cratered terrain of Mercury) have similar Hurst exponents to Eros (0.97 ± 0.01). This suggests that Hurst exponents ~ 1 might be indicative of surfaces dominated by impact cratering. The Hurst exponent for the interior of Shoemaker (a region with fewer impact craters) is 0.64 ± 0.2 giving additional evidence to support the theory that higher Hurst exponents are indicative of surfaces dominated by cratering. Finally, Itokawa, an asteroid with very few obvious craters, (Saito et al., 2006) is not self-affine and a Hurst exponent could not be fit (Barnouin-Jha et al., 2008).

A question does arise to the theory that higher Hurst exponents are indicative of a crater dominated surface when looking at Eros. How can the Hurst exponent be indicative of cratering if the Hurst exponent includes surface roughness values from baselines that are not sensitive to impact cratering (i.e., baselines dominated by boulders)? One explanation of the Hurst exponent continuing to smaller baselines is that block distribution on Eros is a result of cratering and the surface roughness is still fundamentally a function of impact cratering. If the surface is missing one part of this scenario (either blocks or craters) the Hurst exponent decreases, like in Shoemaker ($H = 0.63 \pm 0.02$) where very few craters are present. The Hurst exponent may be indicative of both the crater cavity (at larger baselines) and blocks from the crater's ejecta (at smaller baselines). Another explanation is that the Hurst exponent is not indicative of a single geologic process at all and there is some other reason that the Hurst exponent is similar in multiple terrains that are dominated by cratering. The results of this study cannot provide a definitive answer, but by continuing to measure the surface roughness of different bodies in the solar system we can gather more data to understand what the Hurst exponent says about the origin and evolution of the surfaces of planetary bodies.

5.4. Comparison of surface roughness of Eros from NLR to surface roughness derived from thermophysical models

As mentioned previously, RMS deviation (or the related measure of RMS slope) is used by the thermal inertia community to quantify the surface roughness of asteroids. A previous study has investigated the surface roughness of Eros using thermal-infrared observations and a thermophysical model to calculate RMS slope at a baseline of 0.005 m (Rozitis, 2017). Using the Hurst exponent (and assuming the Hurst exponent stays constant down to the relevant baseline of 0.005 m) we can calculate RMS deviation at 0.005 m to compare the results of this paper to Rozitis (2017). A large caveat to such a comparison is the strong likelihood that the Hurst exponent would vary from baselines of meters to baselines of centimeters. A previous study extrapolated on Mars found that the Hurst exponent differs from baselines of meters to baselines of kilometers due to the different geologic processes controlling surface roughness at such scales (Campbell, 2003). With this caveat in mind, we calculated the surface roughness at a scale of 0.005 m (the scale measured in Rozitis (2017)) using our measurement of the global Hurst exponent and ν_o and found a measure of the surface roughness of 0.082 ± 0.001 m. This compares to the surface roughness measured by Rozitis (2017) of 0.0039 ± 0.001 m. They reported their measurement in RMS slope ($38 \pm 8°$), but RMS slope can be converted into RMS deviation by multiplying tangent of RMS slope by the baseline Shepard et al. (2001). The RMS deviation calculated using our Hurst exponent and the measurement calculated by thermal-infrared observations and thermophysical modeling differs outside each of the respected error bars. The source of this discrepancy is likely the change in Hurst exponent at smaller scales. The Hurst exponent at the baselines measured in our paper is controlled by the interplay of boulders and impact craters producing topography on Eros. At a baseline of centimeters to sub-centimeters different surface processes are controlling topography including regolith size and even the texture of individual regolith grains. Additionally, the age of the surface could control surface roughness at smaller scales since thermal effects and micrometeorites could change the surface roughness at the scale of centimeters. The surface roughness at smaller scales could be driven by different processes which would make a straight downard continuation of the Hurst exponent unlikely for the global surface.

We can investigate the relationship between NLR-derived surface roughness and the thermophysical modeling-derived surface roughness further in two ways. In the first investigation, we can hold the surface roughness measurement from Rozitis (2017) constant and assume the Hurst exponent is constant to small baselines, but allow the baseline of the Rozitis (2017) to change. Using Eqn. (2) we find that a baseline of 0.025 m (2.5 cm) matches both of these criteria. Second, we can assume the Hurst exponent changes at the 1 m baseline, and keep the surface roughness measurement and baseline from Rozitis (2017) constant and find the Hurst exponent that would fit the data. This results in a Hurst exponent of 0.67. Both of these small investigations raise new possibilities. The change of the baseline in the first investigation results in a baseline of surface roughness measurements that could be possible for thermophysical modeling-derived surface roughness, as the baseline the surface roughness is measured over is not as clear as in laser altimeter-derived surface roughness Rozitis and Green (2012). In the second investigation, the changing of the Hurst exponent resulted in a Hurst exponent that has been observed on planetary surfaces (Shepard et al., 2001). The discrepancy between the two datasets will likely only be resolved when high-resolution topographic measurements of asteroids are performed allowing laser altimeter-derived surface roughness to be calculated at centimeter and smaller scale baselines.

6. Conclusion

In this study, we undertook the first global mapping of the meter-scale surface roughness of 433 Eros. The global surface roughness of Eros is self-affine with a Hurst exponent of 0.97 ± 0.01. Boulders and impact craters produce the surface roughness at different scale lengths on Eros, the crater Shoemaker, in particular, has higher surface roughness values relative to the rest of Eros at small baselines (due to the high density of boulders) and low surface roughness values compared to the rest of Eros at large baselines (due to the low density of impact craters). It is likely that a single event, the formation of Shoemaker, shaped the surface roughness of Eros at all baselines measured. Surface roughness is not correlated with tectonic lineaments, ponds, or slope on a global level. The thickness of mobile regolith that infills topography and covers boulders is estimated to be 0.2–6.2 m. By comparing Eros to surface roughness measurements from other bodies in the solar system we suggest that a Hurst exponent of near ~ 1 may be indicative of a surface dominated by impact cratering. The surface roughness (deviogram and Hurst exponent) of Eros is more lunar-like than Itokawa-like suggesting the interior has strength to support larger-scale topography.

Acknowledgments

We would like to thank Gregory Neumann and an anonymous reviewer for helpful comments and suggestions on this paper. We would also like to thank

Oded Aharonson for editorial handling. Finally, we thank C.L. Johnson and K. Lewis for helpful comments on an earlier version of this paper. This work was funded by NASA grant NNX11AQ48G from the Planetary Mission and Data Analysis Program. H.C.M.S. acknowledges the Johns Hopkins Applied Physics Laboratory Graduate Research Fellowship for additional funding. We would like to thank P.C. Thomas for the boulder and crater counts for Eros.

References

Abe, S., Mukai, T., Hirata, N., Barnouin-Jha, O. S., Cheng, A. F., Demura, H., Gaskell, R. W., Hashimoto, T., Hiraoka, K., Honda, T., Kubota, T., Matsuoka, M., Mizuno, T., Nakamura, R., Scheeres, D. J., Yoshikawa, M., Jun. 2006. Mass and local topography measurements of Itokawa by Hayabusa. Science 312 (5778), 1344–1347.

Barnouin, O. S., Gaskell, R. W., Ernst, C. M., May 2012. Revisiting the NEAR-Shoemaker landing site. Asteroids, Comets, Meteors 2012 1667.

Barnouin-Jha, O. S., Baloga, S., Glaze, L., Apr. 2005. Comparing landslides to fluidized crater ejecta on Mars. Journal of Geophysical Research 110 (E), 4010.

Barnouin-Jha, O. S., Cheng, A. F., Mukai, T., Abe, S., Hirata, N., Nakamura, R., Gaskell, R. W., Saito, J., Clark, B. E., Nov. 2008. Small-scale topography of 25143 Itokawa from the Hayabusa laser altimeter. Icarus 198 (1), 108–124.

Benner, L. A. M., Ostro, S. J., Magri, C., Nolan, M. C., Howell, E. S., Giorgini, J. D., Jurgens, R. F., Margot, J.-L., Taylor, P. A., Busch, M. W., Shepard, M. K., Dec. 2008. Near-Earth asteroid surface roughness depends on compositional class. Icarus 198 (2), 294–304.

Buczkowski, D. L., Barnouin-Jha, O. S., Prockter, L. M., Jan. 2008. 433 Eros lineaments: Global mapping and analysis. Icarus 193 (1), 39–52.

Campbell, B. A., 2003. Limits on inference of Mars small-scale topography from MOLA data. Geophysical Research Letters 30 (3), 1116.

Chapman, C. R., Merline, W. J., Thomas, P. C., Joseph, J., Cheng, A. F., Izenberg, N., Jan. 2002. Impact History of Eros: Craters and Boulders. Icarus 155 (1), 104–118.

Cheng, A. F., Barnouin-Jha, O., Prockter, L., Zuber, M. T., Neumann, G., Smith, D. E., Garvin, J., Robinson, M., Veverka, J., Thomas, P., Jan. 2002. Small-Scale Topography of 433 Eros from Laser Altimetry and Imaging. Icarus 155 (1), 51–74.

Cheng, A. F., Barnouin-Jha, O., Zuber, M. T., Veverka, J., Smith, D. E., Neumann, G. A., Robinson, M., Thomas, P., Garvin, J. B., Murchie, S., Chapman, C., Prockter, L., Apr. 2001. Laser altimetry of small-scale features on 433 Eros from NEAR-Shoemaker. Science 292 (5516), 488–491.

Dombard, A. J., Barnouin, O. S., Prockter, L. M., Thomas, P. C., Dec. 2010. Boulders and ponds on the Asteroid 433 Eros. Icarus 210 (2), 713–721.

Fa, W., Cai, Y., Xiao, Z., Tian, W., Apr. 2016. Topographic roughness of the northern high latitudes of Mercury from MESSENGER Laser Altimeter data. Geophysical Research Letters, doi:10.1002–2016GL068120.

Fujiwara, A., Kawaguchi, J., Yeomans, D. K., Abe, M., Mukai, T., Okada, T., Saito, J., Yano, H., Yoshikawa, M., Scheeres, D. J., Barnouin-Jha, O., Cheng, A. F., Demura, H., Gaskell, R. W., Hirata, N., Ikeda, H., Kominato, T., Miyamoto, H., NAKAMURA, A. M., Nakamura, R., Sasaki, S., Uesugi, K., Jun. 2006. The Rubble-Pile Asteroid Itokawa as Observed by Hayabusa. Science 312 (5), 1330–1334.

Garvin, J. B., Frawley, J. J., Abshire, J. B., 1999. Vertical roughness of Mars from the Mars Orbiter Laser Altimeter. Geophysical Research Letters 26 (3), 381–384.

Gaskell, B., 2008. Gaskell Eros Shape Model V1.0. NEAR-A-MSI-5-EROSSHAPE-V1.0. NASA Planetary Data System.

Glaze, L. S., Baloga, S. M., Stofan, E. R., Sep. 2003. A methodology for constraining lava flow rheologies with MOLA. Icarus 165 (1), 26–33.

Harris, A. W., Lagerros, J. S. V., 2002. Asteroids in the Thermal Infrared. In: Bottke, W. F. (Ed.), Asteroids III. Tucson.

Kahn, E. G., Barnouin, O. S., Daly, M. G., Johnson, C. L., Seabrook, J., Mar. 2015. Reconstruction of the Eros Shape Model Using NEAR Laser Rangefinder Data. 46th Lunar and Planetary Science Conference 46, 2874.

Kreslavsky, M. A., Head, J. W., Nov. 2000. Kilometer-scale roughness of Mars: Results from MOLA data analysis. Journal of Geophysical Research: Planets (1991–2012) 105 (E11), 26695–26711.

Kreslavsky, M. A., Head, J. W., Neumann, G. A., 2014. Kilometer-scale topographic roughness of Mercury: Correlation with geologic features and units. Geophysical Research Letters 41, 1–7.

Kreslavsky, M. A., Head, J. W., Neumann, G. A., Rosenburg, M. A., Aharonson, O., Smith, D. E., Zuber, M. T., Oct. 2013. Lunar topographic roughness maps from Lunar Orbiter Laser Altimeter (LOLA) data: Scale dependence and correlation with geologic features and units. Icarus 226 (1), 52–66.

Krishna, N., Kumar, P. S., Jan. 2016. Impact spallation processes on the Moon: A case study from the size and shape analysis of ejecta boulders and secondary craters of Censorinus crater. Icarus 264 (C), 274–299.

Miller, J. K., Konopliv, A. S., Antreasian, P. G., Bordi, J. J., Chesley, S., Helfrich, C. E., Owen, W. M., Wang, T. C., Williams, B. G., Yeomans, D. K., Jan. 2002. Determination of shape, gravity, and rotational state of asteroid 433 Eros. Icarus 155 (1), 3–17.

Miyamoto, H., Yano, H., Scheeres, D. J., Abe, S., Barnouin-Jha, O., Cheng, A. F., Demura, H., Gaskell, R. W., Hirata, N., Ishiguro, M., Michikami, T., Nakamura, A. M., Nakamura, R., Saito, J., Sasaki, S., 2007. Regolith migration and sorting on asteroid Itokawa. Science 316 (5827), 1011–1014.

Murdoch, N., Sánchez, P., Schwartz, S. R., Miyamoto, H., 2015. Asteroid Surface Geophysics. Asteroids IV, 767–792.

Roberts, J. H., Kahn, E. G., Barnouin, O. S., Ernst, C. M., Prockter, L. M., Gaskell, R. W., Oct. 2014. Origin and flatness of ponds on asteroid 433 Eros. Meteoritics & Planetary Science 49 (10), 1735–1748.

Robinson, M. S., Thomas, P. C., Veverka, J., Murchie, S., Carcich, B., 2001. The nature of ponded deposits on Eros. Nature 413 (6854), 396–400.

Robinson, M. S., Thomas, P. C., Veverka, J., Murchie, S. L., Wilcox, B. B., Dec. 2002. The geology of 433 Eros. Meteoritics & Planetary Science 37 (12), 1651–1684.

Rosenburg, M. A., Aharonson, O., Head, J. W., Kreslavsky, M. A., Mazarico, E., Neumann, G. A., Smith, D. E., Torrence, M. H., Zuber, M. T., Feb. 2011. Global surface slopes and roughness of the Moon from the Lunar Orbiter Laser Altimeter. Journal of Geophysical Research 116 (E2), E02001.

Rozitis, B., Jan. 2017. The surface roughness of (433) Eros as measured by thermal-infrared beaming. Monthly Notices of the Royal Astronomical Society 464 (1), 915–923.

Rozitis, B., Green, S. F., Jun. 2012. The influence of rough surface thermal-infrared beaming on the Yarkovsky and YORP effects. Monthly Notices of the Royal Astronomical Society 423 (1), 367–388.

Saito, J., Miyamoto, H., Nakamura, R., Ishiguro, M., Michikami, T., NAKAMURA, A. M., Demura, H., Sasaki, S., Hirata, N., Honda, C., Yamamoto, A., Yokota, Y., Fuse, T., Yoshida, F., Tholen, D. J., Gaskell, R. W., Hashimoto, T., Kubota, T., Higuchi, Y., Nakamura, T., Smith, P., Hiraoka, K., Honda, T., Kobayashi, S., Furuya, M., Matsumoto, N., Nemoto, E., Yukishita, A., Kitazato, K., Dermawan, B., Sogame, A., Terazono, J., Shinohara, C., Akiyama, H., Jun. 2006. Detailed Images of Asteroid 25143 Itokawa from Hayabusa. Science 312 (5), 1341–1344.

Shepard, M. K., Campbell, B. A., Bulmer, M. H., Farr, T. G., Gaddis, L. R., Plaut, J. J., Dec. 2001. The roughness of natural terrain: A planetary and remote sensing perspective. Journal of Geophysical Research 106 (E), 32777–32796.

Susorney, H., Barnouin, O., Ernst, C., Byrne, P., 2017. Surface Roughness of Mercury from MESSENGER. Journal of Geophysical Research - Planets.

Thomas, N., Barbieri, C., Keller, H. U., Lamy, P., Rickman, H., Rodrigo, R., Sierks, H., Wenzel, K. P., Cremonese, G., Jorda, L., Küppers, M., Marchi, S., Marzari, F., Massironi, M., Preusker, F., Scholten, F., Stephan, K., Barucci, M. A., Besse, S., El-Maarry, M. R., Fornasier, S., Groussin, O., Hviid, S. F., Koschny, D., Kührt, E., Martellato, E., Moissl, R., Snodgrass, C., Tubiana, C., Vincent, J. B., Jun. 2012. The geomorphology of (21) Lutetia: Results from the OSIRIS imaging system onboard ESA's Rosetta spacecraft. Planetary and Space Science 66 (1), 96–124.

Thomas, P. C., Joseph, J., Carcich, B., Veverka, J., Clark, B. E., Bell, J. F., Byrd, A. W., Chomko, R., Robinson, M., Murchie, S., Prockter, L., Cheng, A., Izenberg, N., Malin, M., Chapman, C., McFadden, L. A., KIRK, R., Gaffey, M., Lucey, P. G., Jan. 2002. Eros: Shape, topography, and slope processes. Icarus 155 (1), 18–37.

Thomas, P. C., Robinson, M. S., Jul. 2005. Seismic resurfacing by a single impact on the asteroid 433 Eros. Nature 436 (7049), 366–369.

Thomas, P. C., Veverka, J., Robinson, M. S., Murchie, S., 2001. Shoemaker crater as the source of most ejecta blocks on the asteroid 433 Eros. Nature 413 (6854), 394–396.

Turcotte, D. L., Jul. 1997. Fractals and Chaos in Geology and Geophysics. Fractals and Chaos in Geology and Geophysics, Cornell University, New York.

Veverka, J., Robinson, M., Thomas, P., Murchie, S., Bell, J. F., Izenberg, N., Chapman, C., Harch, A., Bell, M., Carcich, B., Cheng, A., Clark, B., Domingue, D., Dunham, D., Farquhar, R., Gaffey, M. J., Hawkins, E., Joseph, J., KIRK, R., Li, H., Lucey, P., Malin, M., Martin, P., McFadden, L., Merline, W. J., Miller, J. K., Owen, W. M., Peterson, C., Prockter, L., Warren, J., Wellnitz, D., Williams, B. G., Yeomans, D. K., Sep. 2000. NEAR at Eros: Imaging and Spectral Results. Science 289 (5487), 2088–2097.

Veverka, J., Thomas, P. C., Robinson, M., Murchie, S., Chapman, C., Bell, M., Harch, A., Merline, W. J., Bell, J. F., Bussey, B., Carcich, B., Cheng, A., Clark, B., Domingue, D., Dunham, D., Farquhar, R., Gaffey, M. J., Hawkins, E., Izenberg, N., Joseph, J., KIRK, R., Li, H., Lucey, P., Malin, M., McFadden, L., Miller, J. K., Owen, W. M., Peterson, C., Prockter, L., Warren, J., Wellnitz, D., Williams, B. G., Yeomans, D. K., 2001. Imaging of small-scale features on 433 Eros from NEAR: Evidence for a complex regolith. Science 292 (5516), 484–488.

Wilkison, S. L., Robinson, M. S., Thomas, P. C., Veverka, J., McCoy, T. J., Murchie, S. L., Prockter, L. M., Yeomans, D. K., Jan. 2002. An Estimate of Eros's Porosity and Implications for Internal Structure. Icarus 155 (1), 94–103.

Zuber, M., Smith, D., Cheng, A., Garvin, J., Aharonson, O., Cole, T., Dunn, P., Guo, Y., Lemoine, F., Neumann, G., Rowlands, D., Torrence, M., Sep. 2000. The shape of 433 eros from the NEAR-shoemaker laser rangefinder. Science 289 (5487), 2097–2101.

Zuber, M. T., Smith, D. E., Cheng, A. F., Cole, T. D., Oct. 1997. The NEAR laser ranging investigation. Journal of Geophysical Research 102 (E), 23761–23774.

Tables

Table 1: Surface roughness values from this study and other studies.

Object	L [m]	$\nu(10)$ [m]	H	
433 Eros	4–200	1.2	0.97 ± 0.01	This study
433 Eros	4-2000	∼1	0.87	Cheng et al. (2001)
25143 Itokawa-Highlands	5-101	1.8	N/A	Barnouin-Jha et al. (2008)
25143 Itokawa-Lowlands	5-101	0.6	N/A	Barnouin-Jha et al. (2008)
Lunar-Mare	60-200	N/A	0.91 ± 0.01	This study
Lunar-Highlands	60-200	N/A	1.00 ± 0.02	This study
Lunar-Mare	17–2500	N/A	0.76	Rosenburg et al. (2011)
Lunar-Highlands	17–2500	N/A	0.95	Rosenburg et al. (2011)
Mercury-Cratered Terrain	500–250000	N/A	0.95 ± 0.01	Susorney et al. (2017)
Mercury-Smooth Plains	500–250000	N/A	0.88 ± 0.01	Susorney et al. (2017)

Figures

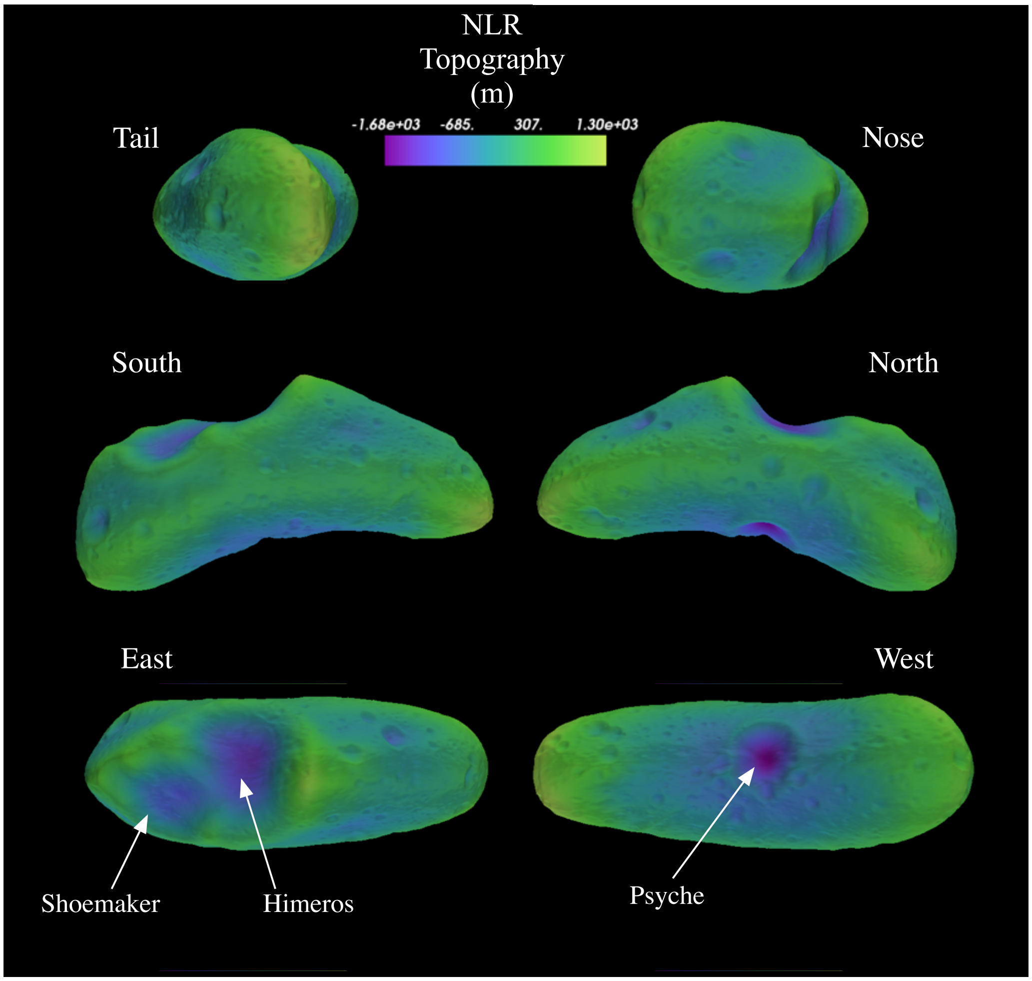

Figure 1: Topography in meters of 433 Eros derived from a shape model (Gaskell, 2008). The topography is derived from a geoid that assumes the interior of Eros is a constant density, see section 2.3 for details. The three largest craters, Himeros (10 km in diameter), Shoemaker (7.6 km in diameter, formally known as Charlios Regio), and Psyche (5.3 km in diameter) are labeled.

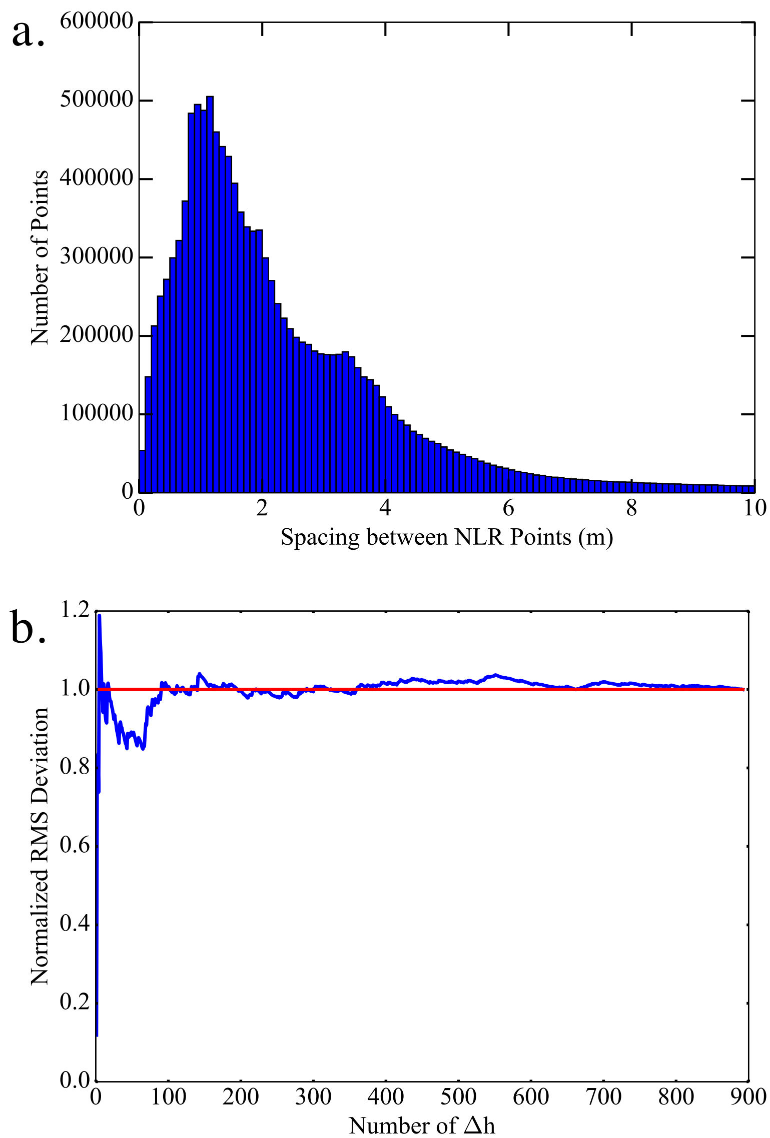

Figure 2: (a) A histogram of the direct-line spacing between NLR tracks. (b) The stability of RMS deviation $\nu(L)$ for a single location on 433 Eros at $L = 100$ m. Normalized RMS deviation is the RMS deviation for the specified number of Δh divided by the final RMS deviation for all Δh.

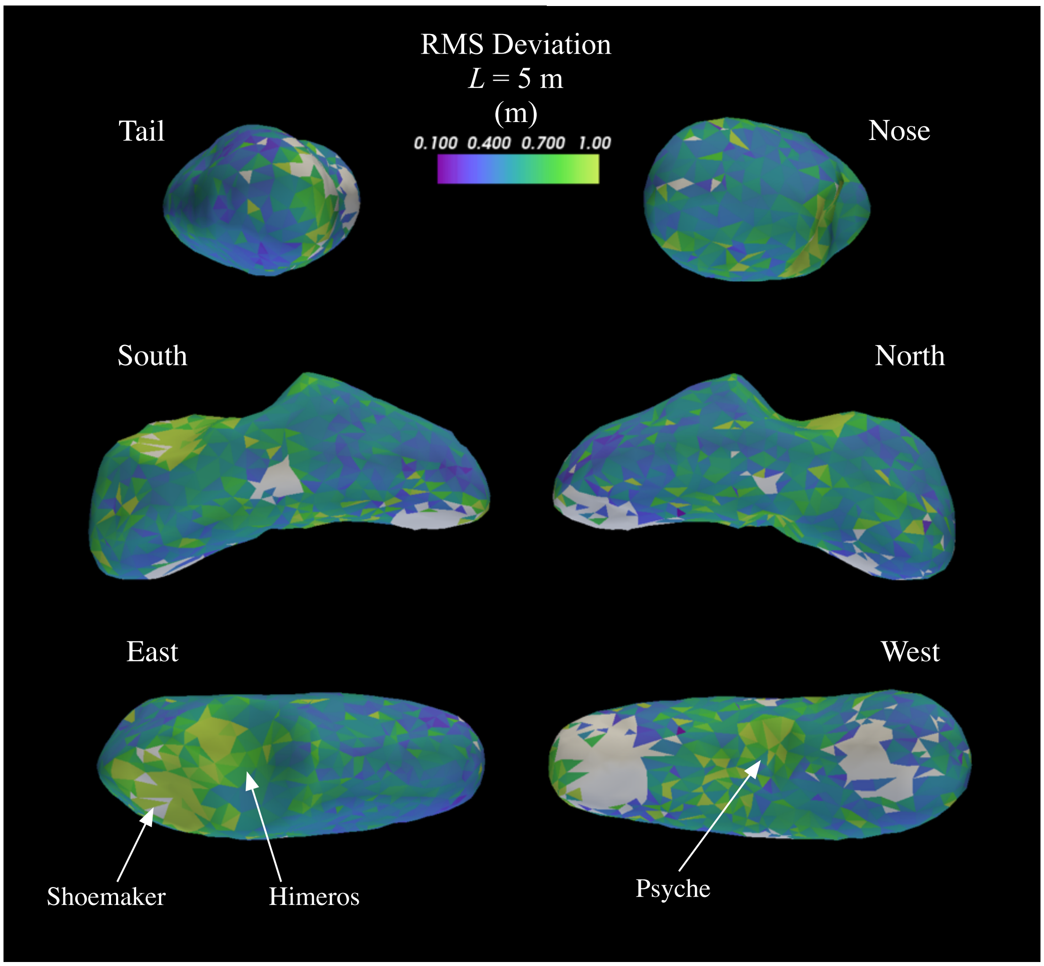

Figure 3: RMS deviation at $L = 5$ m. The surface roughness values are largest in the craters Himeros, Shoemaker, and Psyche.

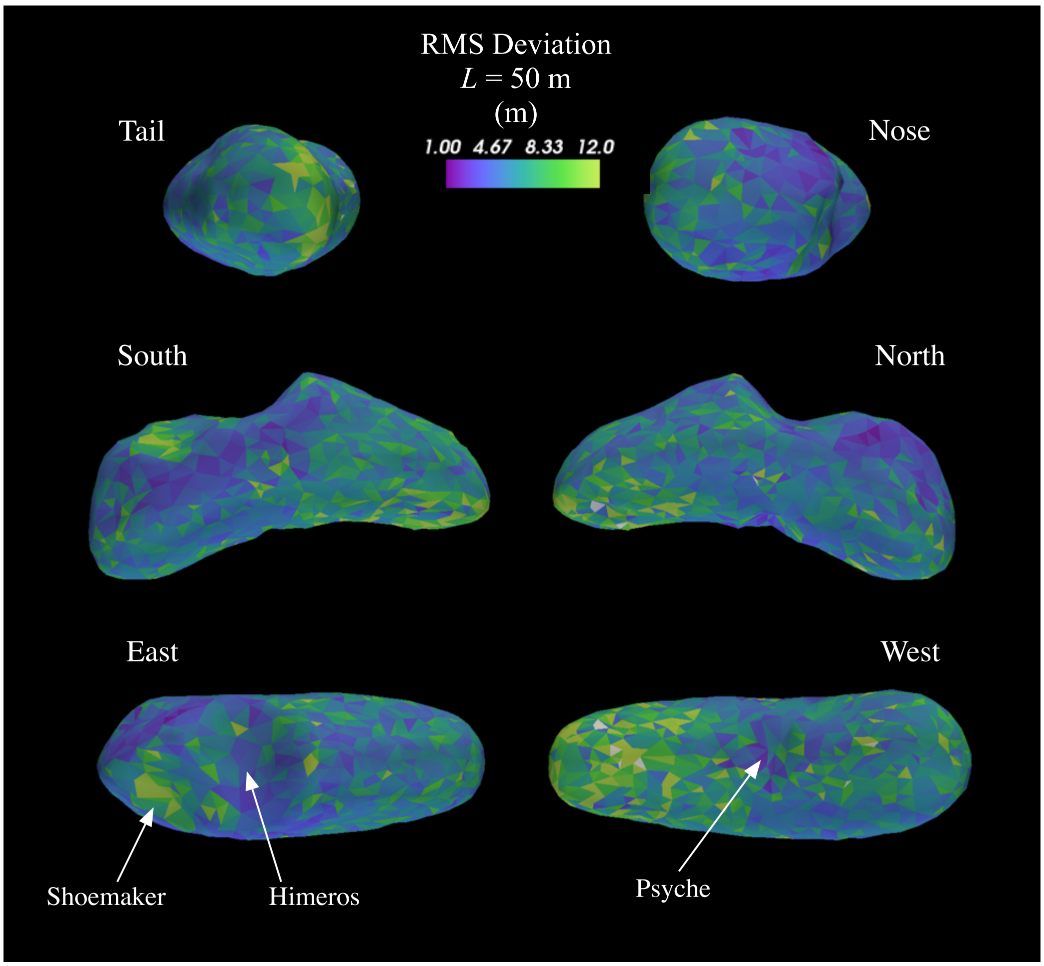

Figure 4: RMS deviation at $L = 50$ m. The surface roughness inside Shoemaker is slightly elevated compared to the surrounding region.

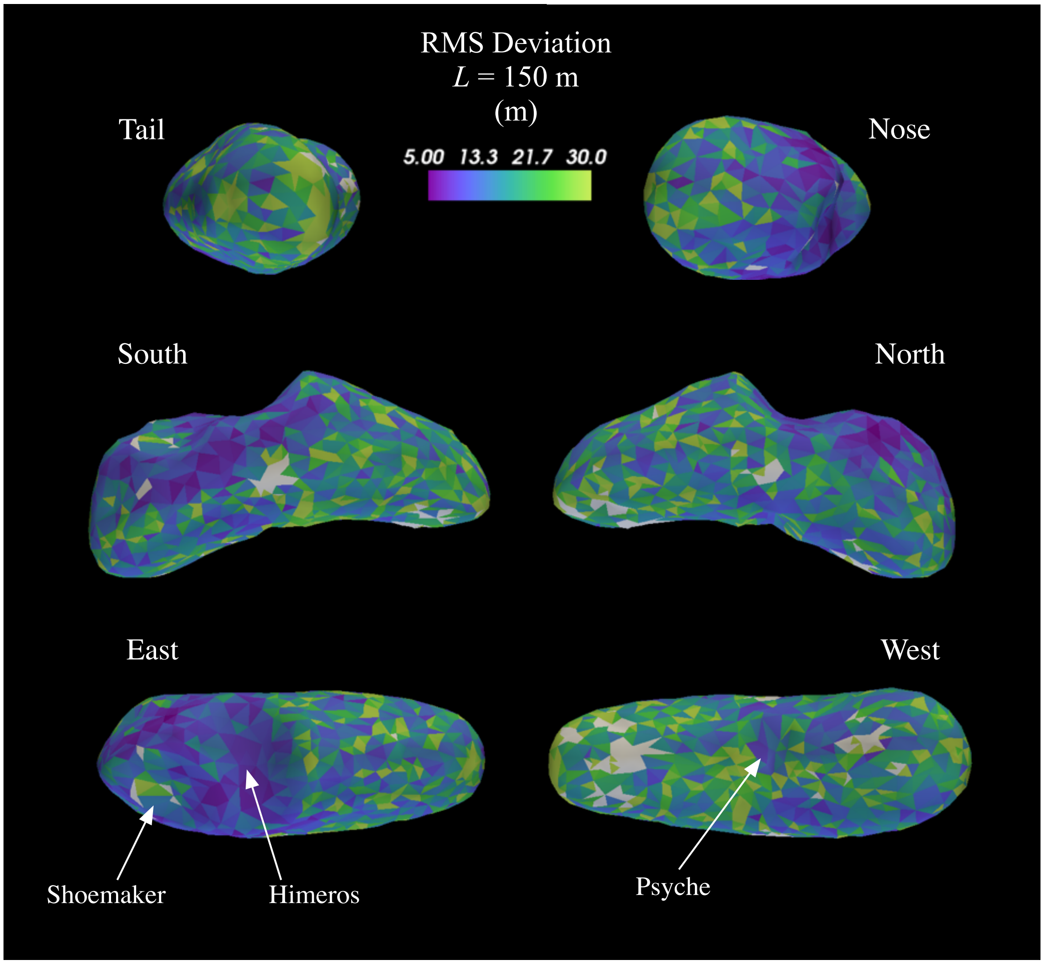

Figure 5: RMS deviation at $L = 150$ m. Low surface roughness values are found within the craters Shoemaker and Himeros.

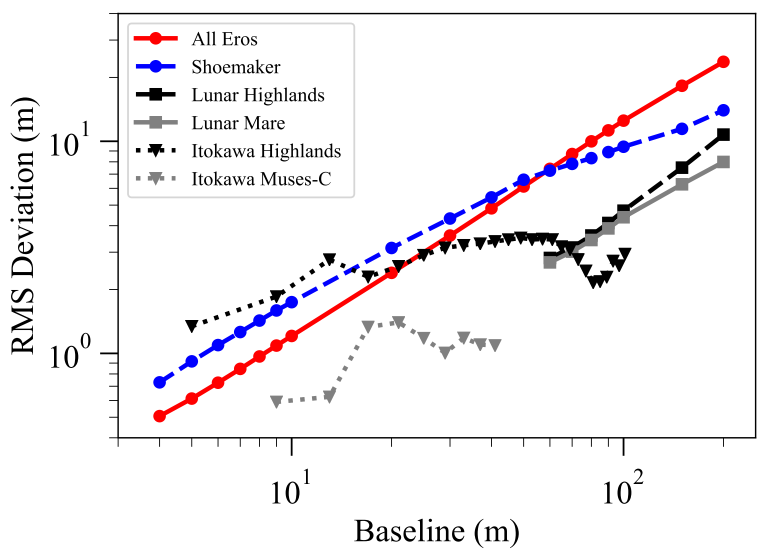

Figure 6: A deviogram of 433 Eros that shows the global deviogram of Eros ('All Eros'), a deviogram of Shoemaker (all surface roughness measurements within the rim of Shoemaker), a deviogram of the lunar highlands, a deviogram of the lunar mare, and surface roughness measurements from Itokawa's lowlands and highlands. The deviograms of the moon were calculated by the authors for this study. The surface roughness measurements of Itokawa are from Barnouin-Jha et al. (2008).

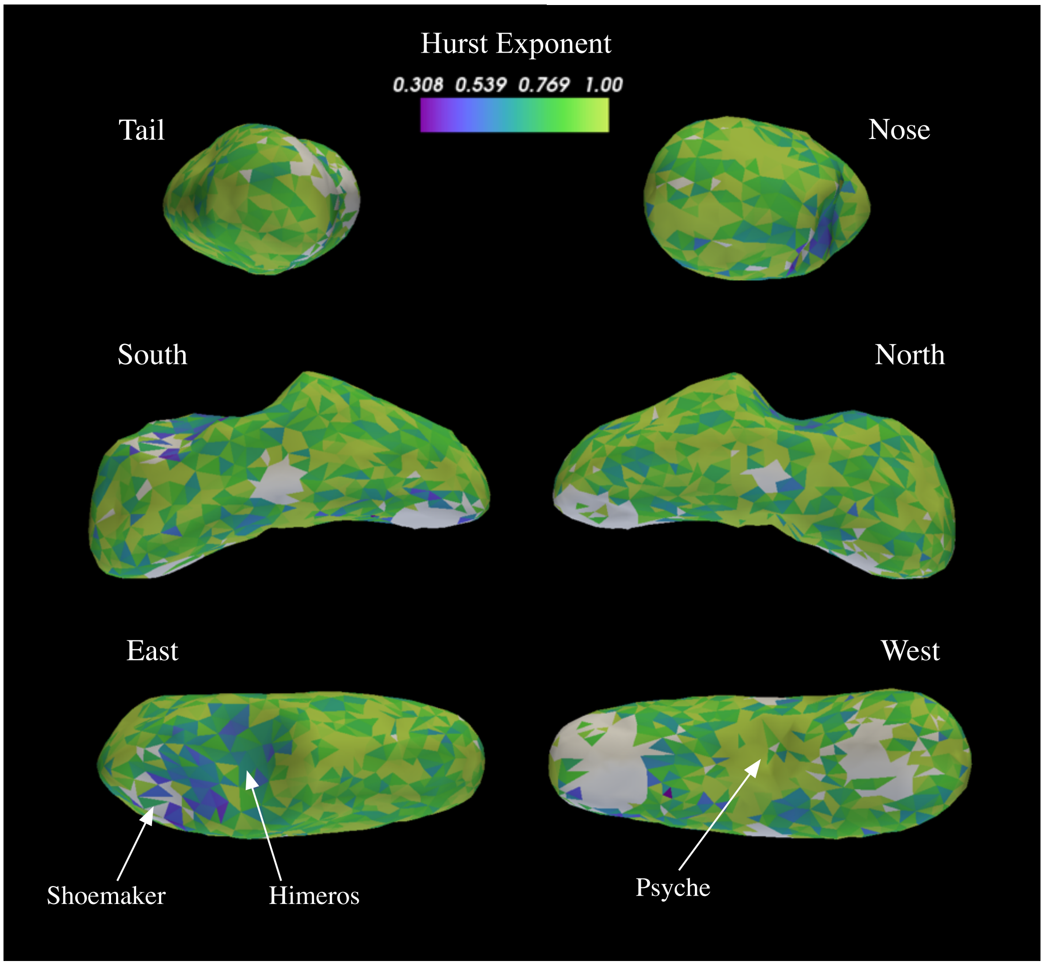

Figure 7: Map of the Hurst exponents calculated for each plate. Hurst exponents are lowest with the craters Shoemaker and Himeros and ~ 1 in Psyche.

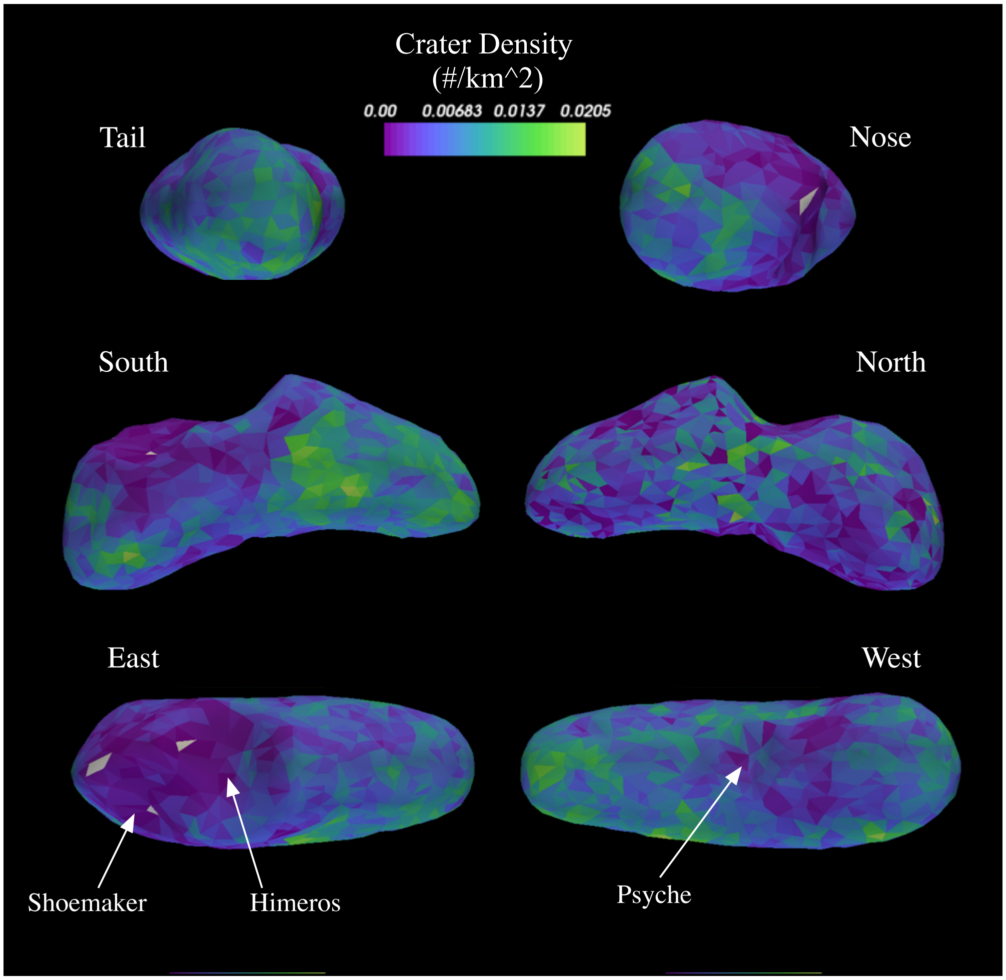

Figure 8: Crater density from Thomas and Robinson (2005). The lowest crater density is found in the craters Shoemaker and Himeros.

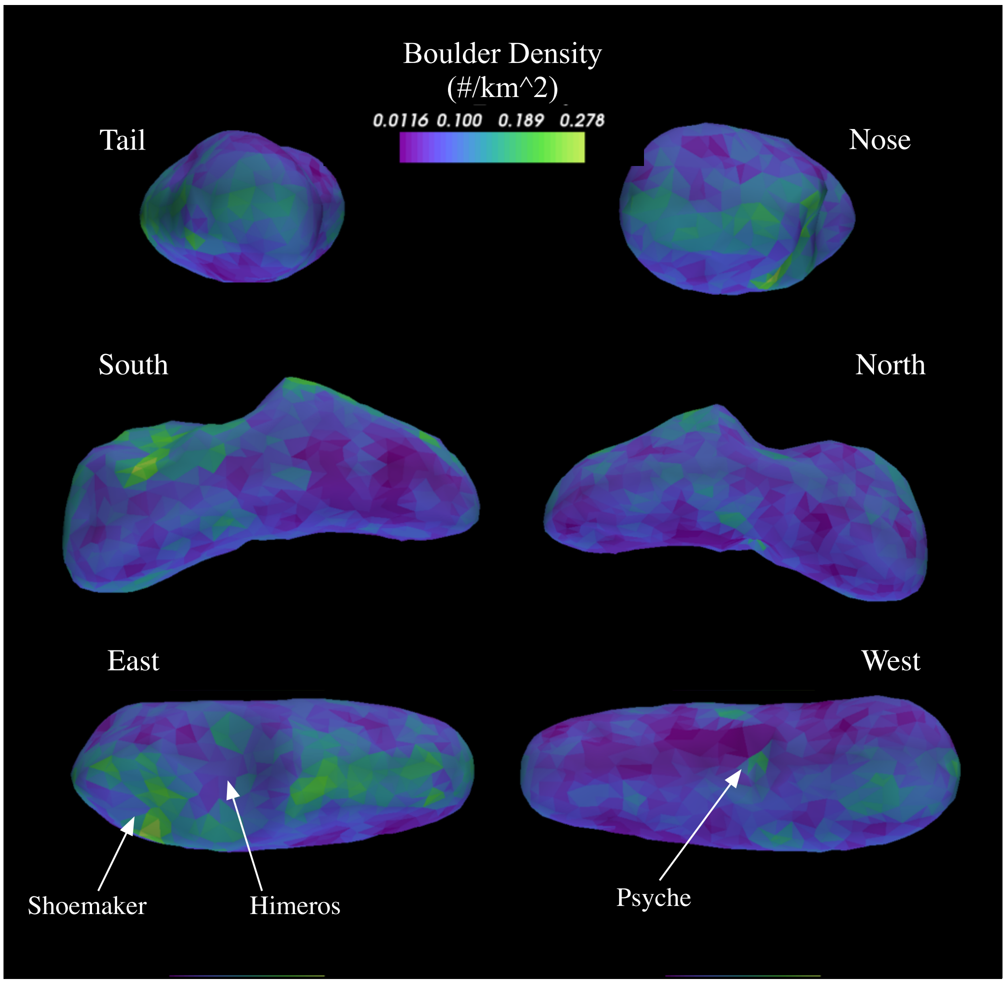

Figure 9: Boulder density from Thomas et al. (2002). The highest boulder density is in the crater Shoemaker.

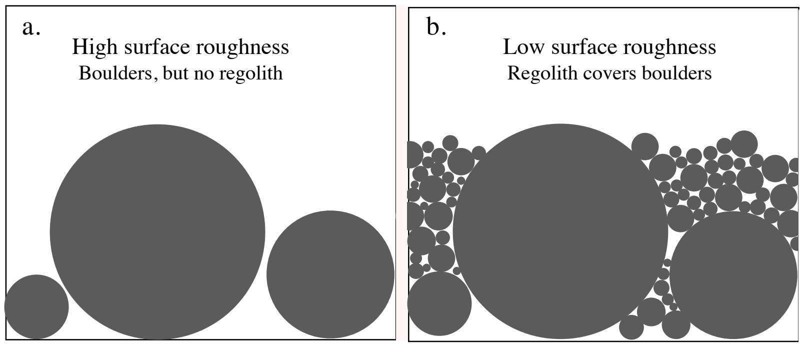

Figure 10: Schematics to show surface roughness in a boulder terrain that either (a) lacks regolith or (b) is covered by regolith.

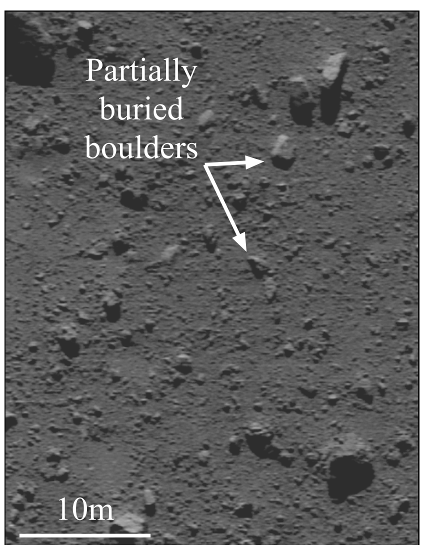

Figure 11: Image of the surface of Eros from the NEAR Multi-Spectral Imager on the southern rim of the crater Himeros. This is one of the highest resolution image of Eros ($\sim$ 0.1 m per pixel resolution). The arrows identify boulders that are buried to different degrees by regolith, similar to observations reported in Veverka et al. (2001).